1,4,5-Trisubstituted Imidazole-Based p53-MDM2/MDMX Antagonists with Aliphatic Linkers for Conjugation with Biological Carriers

Twarda-Clapa, Aleksandra; Krzanik, Sylwia; Kubica, Katarzyna; Guzik, Katarzyna; Labuzek, Beata; Neochoritis, Constantinos G.; Khoury, Kareem; Kowalska, Kaja; Czub, Miroslawa; Dubin, Grzegorz

Published in:
Journal of Medicinal Chemistry

DOI:
10.1021/acs.jmedchem.7b00104

Journal of Medicinal Chemistry

Article

pubs.acs.org/jmc

1,4,5-Trisubstituted Imidazole-Based p53−MDM2/MDMX Antagonists with Aliphatic Linkers for Conjugation with Biological Carriers

Aleksandra Twarda-Clapa,[†,#] Sylwia Krzanik,[†,#] Katarzyna Kubica,[‡,#] Katarzyna Guzik,[‡] Beata Labuzek,[‡] Constantinos G. Neochoritis,[§] Kareem Khoury,[§] Kaja Kowalska,[∥] Miroslawa Czub,[‡] Grzegorz Dubin,[†,⊥] Alexander Dömling,[§] Lukasz Skalniak,*[,‡] and Tad A. Holak*[,‡,∥,⊥]

[†]Faculty of Biochemistry, Biophysics, and Biotechnology, Jagiellonian University, Gronostajowa 7, 30-387 Cracow, Poland

[‡]Faculty of Chemistry, Jagiellonian University, Ingardena 3, 30-060 Cracow, Poland

[§]Department of Drug Design, University of Groningen, Antonius Deusinglaan 1, 9700 AD Groningen, The Netherlands

[∥]Max Plank Institute for Biochemistry, Am Klopferspitz 18, 82152 Martinsried, Germany

[⊥]Malopolska Centre of Biotechnology, Jagiellonian University, Gronostajowa 7a, 30-387 Cracow, Poland

Supporting Information

ABSTRACT: The tumor suppressor protein p53, the "guardian of the genome", is inactivated in nearly all cancer types by mutations in the *TP53* gene or by overexpression of its negative regulators, oncoproteins MDM2/MDMX. Recovery of p53 function by disrupting the p53−MDM2/MDMX interaction using small-molecule antagonists could provide an efficient nongenotoxic anticancer therapy. Here we present the syntheses, activities, and crystal structures of the p53−MDM2/MDMX inhibitors based on the 1,4,5-trisubstituted imidazole scaffold which are appended with aliphatic linkers that enable coupling to bioactive carriers. The compounds have favorable properties at both biochemical and cellular levels. The most effective compound **19** is a tight binder of MDM2 and activates p53 in cancer cells that express the wild-type p53, leading to cell cycle arrest and growth inhibition. Crystal structures reveal that compound **19** induces MDM2 dimerization via the aliphatic linker. This unique dimerization-binding mode opens new prospects for the optimization of the p53−MDM2/MDMX inhibitors and conjugation with bioactive carriers.

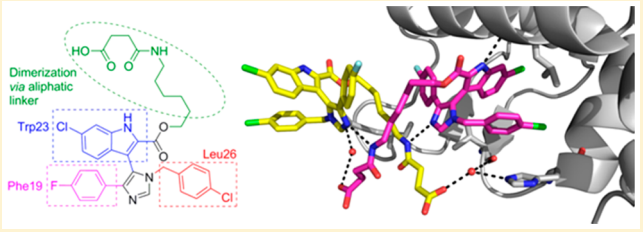

INTRODUCTION

The tumor suppressor p53 is inactivated in the majority of human cancers, which is accomplished either by mutations in the *TP53* gene or by overexpression of p53 negative regulators, primarily MDM2 and/or MDMX.[1−4] Restoration of the function of p53 has been suggested as a promising strategy against cancer.[1,2,5] Mutations in the p53-encoding gene are found in about half of all human cancers and may be combated by gene therapy.[6] In the remaining 50% of cancer cases, in which wild-type p53 ($p53^{wt}$) is present, restoration of its activity by disrupting the interaction with MDM2/X proteins could be achieved by the use of small-molecule antagonists of the MDM2/MDMX−p53 interaction. It has been shown that such antagonists induce p53 downstream proteins, including p21, which leads to the induction of the G0/G1 and G2/M cell cycle arrests and additionally induction of apoptosis in some cancer cell types.[7−10] Such an approach promises a broad range nongenotoxic therapy.[1,11] Several classes of small-molecule MDM2 antagonists entered clinical trials.[3,12−15] However, there are many challenges before entering clinical practice, mainly concerning pharmacological properties, and a constant progress is needed to improve the potency of the compounds and provide precise targeting of cancer cells.[16−19]

The interaction of the N-terminal domain of MDM2 and MDMX with the N-terminal transactivation domain of p53 is mediated by three key side chains of p53 α-helix: Phe19, Trp23, and Leu26, which occupy hydrophobic subpockets on the MDM2 or MDMX surface.[20,21] These interactions form a three-finger pharmacophore, which is present in the most of the currently available small-molecule MDM2 inhibitors.[22,23] Apart from this canonical binding mode, several new approaches were recently proposed,[24,25] for instance, utilizing the transient states of MDM2 for the design of the small molecules occupying yet another, fourth subpocket within MDM2 (inhibitor YH300, 3-(2-(*tert*-butylamino)-1-(*N*-(4-(4-chlorobenzyloxy)benzyl)-formamido)-2-oxoethyl)-6-chloro-1*H*-indole-2-carboxylic acid).[26] A promising class of the p53-based stapled peptides have been recently proposed as another novel group of antagonists.[27,28]

Received: January 20, 2017
Published: May 8, 2017

DOI: 10.1021/acs.jmedchem.7b00104
J. Med. Chem. 2017, 60, 4234−4244

Table 1. Inhibitory Activities of Compound 1 and Its Derivatives against the p53−MDM2/MDMX Interaction Using the FP Assay[a]

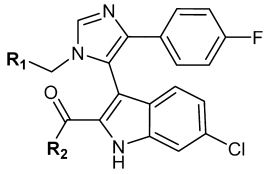

Code	R_2	K_i M2 [μM]	K_i MX [μM]	Code	R_2	K_i M2 [μM]	K_i MX [μM]
1*		0.006	3.15	13	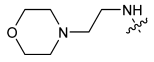	0.121	n.a.#
2	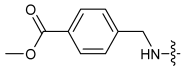	0.225	n.a.	14	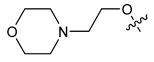	0.017	40.2
3	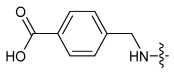	0.023	14.7	15		0.059	n.a.
4	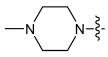	0.038	29.6	16	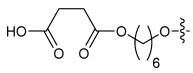	0.015	9.75
5	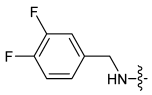	2.31	n.a.	17	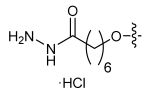	0.098	n.a.
6	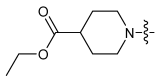	0.038	n.a.	18	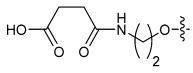	0.054	12.4
7	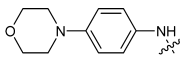	28.0	n.a.	19	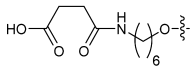	0.058	26.3
8	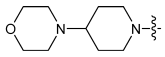	0.008	35.3				
9	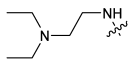	0.656	27.4				
10	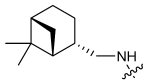	n.a.	n.a.				
11	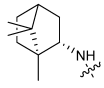	n.a.	n.a.				
12	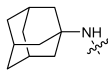	n.a.	n.a.				

Code	R_1	K_i M2	K_i MX
20a±	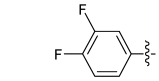	6.02	n.a.
20°		0.021	4.91
21a	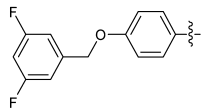	n.a.	n.a.
21		0.060	4.40
22a	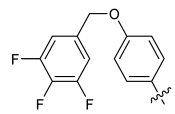	n.a.	n.a.
22		0.433	4.71
23a	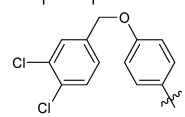	n.a.	n.a.
23		0.322	6.76
24a	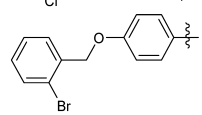	n.a.	n.a.
24		0.157	4.17

[a](*) Compounds **1**−**19** have 4-chlorophenyl group in R_1 position; (○) compounds **20**−**24** have hydroxyl group in R_2 position; (±) **a** is for the ethyl ester (**20a**−**24a**) of the respective acidic forms of **20**−**24**; (#) n.a., not active.

Previously, we reported a novel compound based on an imidazole scaffold (6-chloro-3-(1-(4-chlorobenzyl)-4-phenyl-1*H*-imidazol-5-yl)-1*H*-indole-2-carboxylic acid, WK23, named hereafter **1.1**) and capable of disrupting the MDM2−p53 interaction in vitro.[29] In the present study, we characterize compound **1** (Table 1), a derivative of **1.1**. Compared to **1.1**, the derivatives of **1** have stronger binding to MDM2 and the improved p53-activating and growth-inhibitory activities in cell-based assays. We also report a series of modifications of **1** with aliphatic linkers at the carboxylic group that is attached to the

DOI: 10.1021/acs.jmedchem.7b00104
J. Med. Chem. 2017, 60, 4234−4244

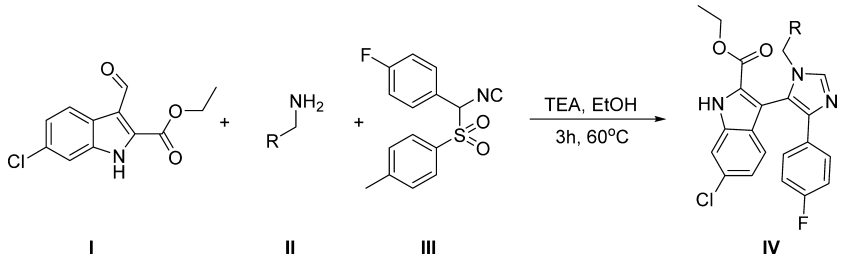

Figure 1. Van Leusen reaction used for the synthesis of the series scaffold. The substituents are varied by changing the amine and isocyanide components (for details, see the Supporting Information).

indole ring system (Table 1). This further improves biological properties of the derivatives of **1**. Our structure-based analysis suggests the potential use of such aliphatic groups for conjugation of the compounds with biological carriers to improve solubility, stability, and precise targeting to malignant neoplasms.

RESULTS AND DISCUSSION

Optimization of Compound 1. In a previous study, we identified **1** as one of the most potent derivatives of **1.1** in disrupting the p53/MDM2 interaction in in vitro biochemical assays.[29] Here we evaluate the activity of **1** in the cells and optimize its p53-activation, growth-inhibitory, and cell-cycle arrest properties by decorating the **1** scaffold (Table 1).

Analyzing the cocrystal structure of **1.1** with MDM2, we identified position R_2 as a potential site for compound expansion. The substituents at this position should point away from the MDM2 molecule, allowing for attachment of solubility/permeability enhancing moieties or linkers for conjugation with targeting biological molecules without significantly affecting the affinity. Such assumptions were tested in compounds **13**−**19**.

1 was obtained in the three-component (3CR) van Leusen reaction (Figure 1).[30] Position R_2 was modified to obtain both amide (**2**−**13**) and ester (**14**−**19**) derivatives using classical chemistry (Supporting Information, Schemes S1−S2, Tables S3−S4). Amide derivatives included two kinds of substituents, polar groups expected to improve the pharmacokinetic properties of **1** and aliphatic moieties tested to evaluate if additional binding at the surface of MDM2 may be obtained. Ester derivatives included aliphatic linkers containing terminal reactive group envisioned for future conjugation with biological carriers/targeting molecules. The binding of selected derivatives was initially tested by NMR titration[31,32] and affinities (K_i) of all evaluated derivatives were tested by fluorescence polarization (FP) assay (Table 1, plots presented in Supporting Information, Table S5).

Different modifications at R_2 position had different effects on the affinity toward MDM2, demonstrating that even though this substituent predictably should point away from the protein molecule, certain moieties were still poorly accepted. Modification with 4-morpholinopiperidinyl (**8**), 2-morpholinoethyl (**14**), or 6-succinyloxyhexyl (**16**) showed no negative effect on affinity. The binding of **3**, **4**, **6**, **18**, and **19** was slightly negatively affected, but the effect was negligible. The effect of other moieties was more pronounced, with the affinities increasing above two-digit nanomolar range (e.g., **2**, **5**, **7**, **9**, and **13**). Bulky substituents were not accepted at all at R_2 position (**10**−**12**). Both tested modification chemistries (amide vs ester) were compatible with MDM2 binding (e.g., **8** and **14**), although particular substituents favored certain chemistries as demonstrated by an order of magnitude better affinity of **14** compared to **13**. Because the modifications were introduced primarily with the aim of improving the effect of compounds on cells, all the derivatives in which affinity was not significantly negatively affected were further evaluated in cellular assay as described below.

Potency of tested compounds toward MDMX followed the trend established for MDM2, although the affinities toward the former protein were around 3 orders of magnitude lower than those toward the latter as previously observed for **1.1**. **1** was the most potent MDMX binder with affinity (K_i) of 3.15 μM. Clearly, despite significant homology of MDM2 and MDMX, subtle differences in their p53 binding pockets[33] preclude optimization of **1** scaffold for concurrent binding to both those proteins.

Bista et al. have demonstrated that extending the Leu26-mimicking substituent within the three-finger pharmacophore in the context of a 6-chloroindole scaffold opens an inducible noncanonical pocket by constraining Tyr100 in a position beneficial for binding larger substituents. Such a four-pocket binding mode was associated with improvement of affinity.[26] Here we tested if similar advantageous effect may be obtained within **1** scaffold. To this end, we introduced elongated benzyl amines in position R_1. These modifications (**21**−**24**) resulted in significant reduction of affinity toward MDM2, demonstrating that **1** scaffold is not suited for exploring the noncanonical pocket observed by Bista et al.[26] Interestingly, in this particular group of compounds, the drop of affinity toward MDM2 was not associated with significant change in potency against MDMX, again demonstrating differences in the p53 binding pockets of those two proteins.

In parallel, we evaluated the affinity of ethyl ester precursors (Supporting Information, Table S2) of the **20**−**24** series, but these compounds (**20a**−**24a**) have entirely lost their affinity both toward MDM2 and MDMX. This is relatively surprising given that the R_2 position is modified with much larger substituents in **13**−**19**, but this phenomenon was not further evaluated in systematic manner.

Derivatives of Compound 1 Induce p53-Target Genes and Arrest the Cell Cycle. The on-target effect of our 1,4,5-trisubstituted imidazoles in a biological context of a living cell was evaluated by assessing the expression level of p53, MDM2, and p21 proteins, which are the products of well-established p53 target genes. All compounds that had K_i values in the FP assay lower than 2 μM were tested. The second-generation MDM2 antagonist RG7388 (Roche; 4-{[(2*R*,3*S*,4*R*,5*S*)-3-(3-chloro-2-fluoro-phenyl)-4-(4-chloro-2-fluorophenyl)-4-cyano-5-(2,2-dimethyl-propyl)-pyrrolidine-2-carbonyl]-amino}-3-methoxybenzoic acid, named hereafter **2.1**)[34] was used as a positive control. **2.1** induced expression of all of the three

DOI: 10.1021/acs.jmedchem.7b00104
J. Med. Chem. 2017, 60, 4234−4244

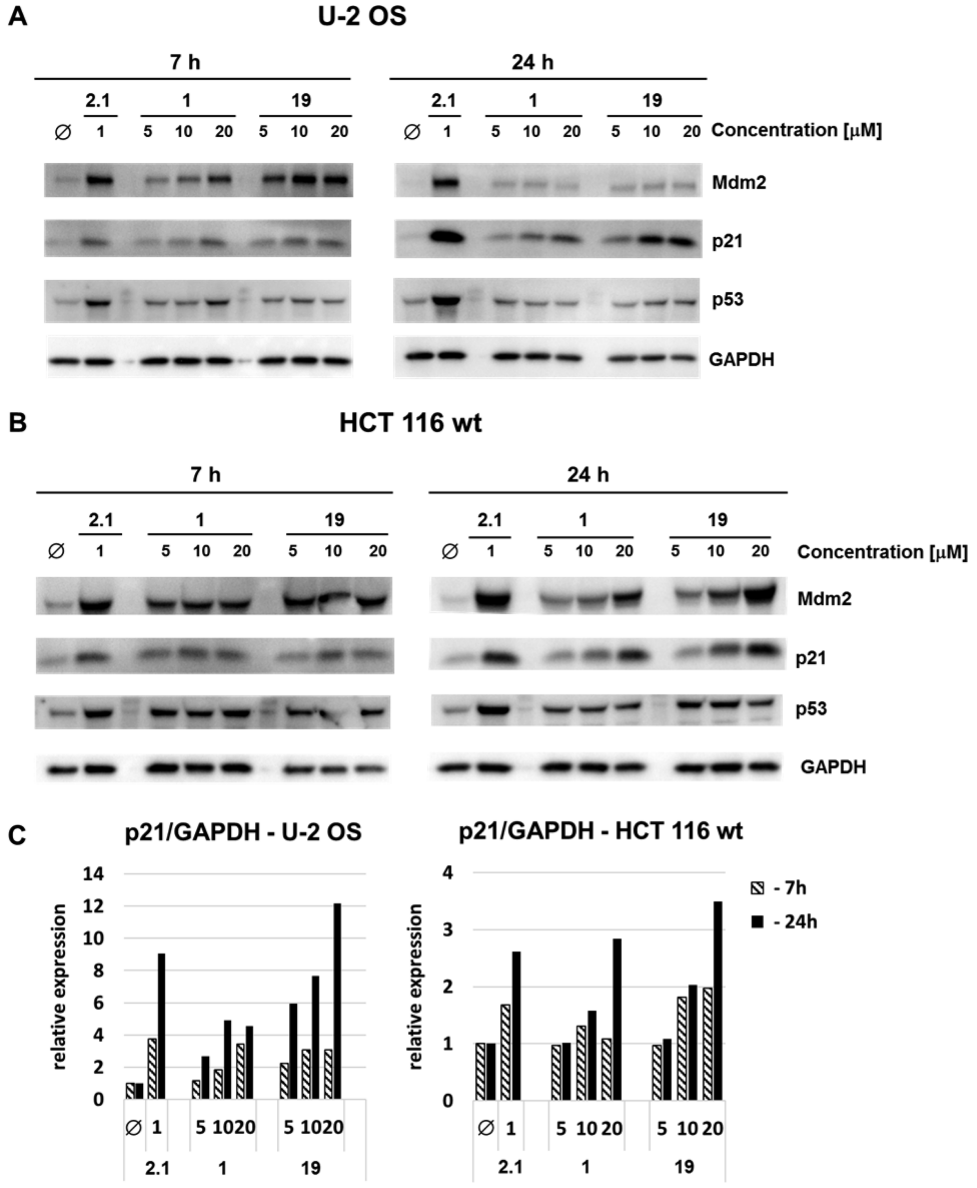

Figure 2. Accumulation of products of the p53 gene and p53-regulated genes upon treatment of cells with the selected compounds. (A,B) The U-2 OS cells and HCT 116 cells (both $p53^{wt}$) were treated with 5, 10, or 20 μM of the indicated compounds for 7 or 24 h. Expression levels of MDM2 and p21 were assessed by Western blot analysis. The GAPDH level served as a protein loading control. (C) Densitometry analysis of the results shown in A and B. Values were normalized to the GAPDH level and to the DMSO-treated control.

proteins already 7 h after the treatment (Figure 2A,B). The densitometry analysis revealed that the level of p21 expression was increased even stronger after 24 h of the treatment (Figure 2C). Out of the tested compounds, **1**, **13**, **14**, **15**, **16**, and **19** induced accumulations of p53, MDM2 and p21, suggesting the activation of the p53 pathway (Figures 2A,B, Supporting Information, Figure S1). From these compounds, only for **13**, **14**, and **19** the induction of p21 expression was further increased at 24 h of the treatment as observed for **2.1**, possibly reflecting improved stability, retention, or activity of the compounds in the cells (Figure 2C).

In parallel, the off-target effects/general toxicity were assessed by comparing the influence of tested agents on the viability of $p53^{wt}$ U-2 OS and p53-null Saos-2 cells. Accordingly, the compounds most active in the Western blot analysis induced growth inhibition of U-2 OS ($p53^{wt}$) cells at lower concentrations than the Saos-2 ($p53^{-/-}$) cells, suggesting on-target effect (Table 2). Compound **15** revealed high toxicity toward Saos-2 cells and was removed from further analysis. As a control, nutlin-3 was used in the MTT assay, confirming its

Table 2. Selectivity of the Tested Compounds toward the p53 Positive Cells[a]

code	U-2 OS IC_{50} [μM]	Saos-2 IC_{50} [μM]	selectivity
19	11.08 ± 1.83	38.56 ± 3.61	3.48
1	17.42 ± 3.49	55.82 ± 13.49	3.20
16	5.71 ± 1.39	12.73 ± 2.66	2.23
13	3.67 ± 0.28	7.15 ± 1.33	1.95
14	7.27 ± 0.63	11.69 ± 1.30	1.61
Nutlin-3	2.66 ± 0.39	20.16 ± 4.71	7.59

[a] IC_{50} values were obtained from the MTT assay. Selectivity is calculated as a ratio of IC_{50} values toward the p53 negative (Saos-2) and positive (U-2 OS) cells.

DOI: 10.1021/acs.jmedchem.7b00104
J. Med. Chem. 2017, 60, 4234−4244

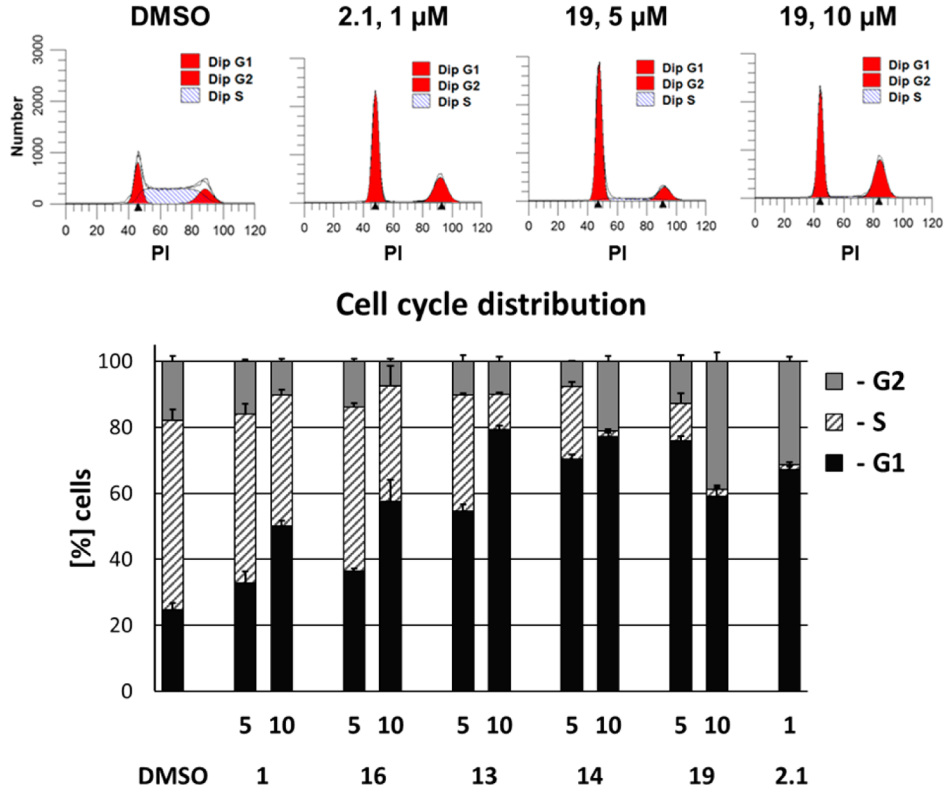

Figure 3. Compound **19** induces cell cycle arrest in the U-2 OS ($p53^{+/+}$) cells. The cells were treated with DMSO, 5 or 10 μM of the tested compounds, or with 1 μM of **2.1** (positive control) for 24 h. The cells were fixed and stained with propidium iodide, followed by flow cytometry analysis of DNA content. Upper panel: exemplary histograms. Lower panel: cell cycle distribution shown as the mean ± SD of two independent experiments.

selectivity toward the $p53^{wt}$ cells (Table 2). The remaining tested compounds were disqualified due to their weak impact on the growth of the U-2 OS cell line (IC_{50} values above 30 μM, e.g., **3**, **18**, or **20**) or high toxicity toward the Saos-2 cells (selectivity lower than 1.5, e.g. **2**, **6**, or **15**).

Accumulation of p21 upon activation of p53 is expected to trigger cell cycle arrest in the $p53^{wt}$ cells. The effect of the five most potent compounds on the cell cycle progression was tested in U-2 OS cells. Treatment with the 5 μM concentration of **13**, **14**, or **19** resulted in a markedly decreased S-phase and increased G1 fraction (Figure 3). At higher concentrations (10 μM), **14** and **19** resulted in nearly complete depletion of the S-phase compartment, while for **1**, **16**, and **13** the increase of the G1 fraction, in the expense of S phase, was clearly observed (Figure 3). The observed extent of cell cycle arrest was comparable to that obtained using 1 μM **2.1**, a compound currently undergoing clinical trials.

Clearly, the selected compounds show the potency in blocking the progression of the cell cycle in a p53-dependent manner, and addition of the 2-morpholinoethyl or, especially, 6-succinyloxyhexyl substituent at position R_2, is profitable for the biological activity of compound **1**. In conclusion, compound **19** presents the best biological properties, as demonstrated by strong and sustained activation of p53-dependent expression of p21, the highest selectivity in the MTT assay, and the strongest induction of cell cycle arrest of $p53^{wt}$ cells.

Crystal Structure of MDM2−19 Complex Reveals Compound Induced Dimerization. To better understand the structural basis of the interactions of evaluated compounds at the binding pocket of MDM2, we determined the crystal structure of **19** in complex with the p53 binding domain of MDM2(18−125) (construct of MDM2 comprising residues 18−125). **19** was selected as the most efficient, cell-available, p53-activating derivative. At the same time, the compound is potentially directly suitable for further conjugation with biological carriers for its reactive group at a long aliphatic linker.

The crystals diffracted to the 1.85 Å resolution and contained four protein molecules in the asymmetric unit. Each protein contained a single inhibitor molecule, all of which were well-defined by their respective electron densities (Supporting Information, Figure S2). No additional inhibitor molecules were found within the structure. In each case, the inhibitor locates at the p53 binding pocket and occupies all the subpockets (Phe19, Trp23, and Leu26) of a canonical three-finger pharmacophore (Figure 4). The interaction of **19** with MDM2 is defined primarily by hydrophobic contacts. The 6-chloroindole substituent inserts into tryptophan pocket and assumes an orientation almost identical to the indole side chain in the native p53−MDM2 complex, while the chlorine atom potentiates the interaction at the bottom of the binding pocket. Further comparable to p53 interaction, the nitrogen within 6-chloroindole participates in a hydrogen bond with the carbonyl oxygen of Leu54. As such, the overall arrangement of 6-chloroindole moiety follows a classical binding observed in a large number of MDM2 inhibitors of different classes and repeating the indole interaction involved in p53 binding.[16] The 4-chlorobezyl substituent fills the Leu26 pocket in an orientation in which the chlorine atom points toward Tyr100. The Phe19 pocket accommodates the 4-fluorophenyl ring directed at Tyr67. The imidazole scaffold of **19** further contributes to the interaction by forming hydrophobic contacts

DOI: 10.1021/acs.jmedchem.7b00104
J. Med. Chem. 2017, 60, 4234−4244

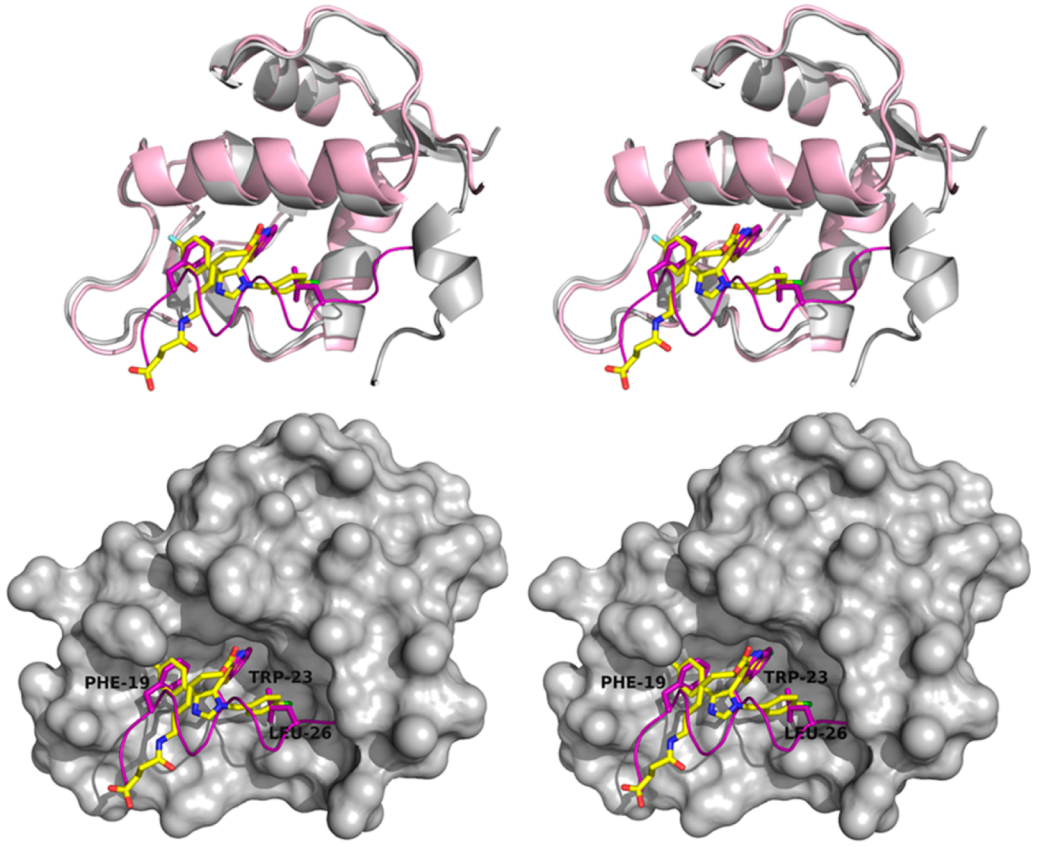

Figure 4. Interaction of MDM2 (residues 18−125) with **19** in comparison with the MDM2−p53 peptide complex (PDB 1YCR). Stereoviews in cartoon (upper panel) or surface representations (lower panel) are shown. MDM2 from the MDM2−**19** complex is shown in gray whereas from the MDM2−p53 complex in pink. **19** is shown as yellow sticks and the p53 peptide as a violet ribbon with the three key interacting amino acids depicted as sticks.

with Val93. As such, the binding of the core of the compound and aromatic substituents is almost identical to that previously described for **1.1**. This is not surprising because **1.1** is a precursor of **19** (Supporting Information, Figure S3).

Most interesting are the interactions of the aliphatic linker unique to **19**. Comparable affinities of **1** and **19** did not portend any pronounced protein−linker interactions. In fact, in the crystal structure the linker protrudes outside the binging pocket. Only the disposition of Gln72 and His73 side chains differs from that observed in **1.1** containing structure. This adjustment is necessary to accommodate the linker (Supporting Information, Figure S3). Remarkably, however, the protruding linker immediately contacts a second inhibitor molecule located within the adjacent MDM2 molecule. The interaction is reciprocal, as the linker of the inhibitor molecule within the pocket of the adjacent MDM2 in turn contacts the inhibitor molecule within the first MDM2. As such, the two MDM2 molecules form a dimer build around a dimer of two inhibitor molecules (Figure 5A,B). The primary contacts between the inhibitor molecules involve hydrogen bonds between the imidazole ring nitrogens and the nitrogens within the aliphatic linker (Figure 5C). The overall dimer is further stabilized by reciprocal intra-MDM2 hydrogen bonds formed by Gln59 and Thr63 (Figure 5D). Moreover, the oxygen from the carboxylic group terminating the aliphatic linker of each **19** molecule forms a water-mediated contact with the side chains (Gln72, His96) of MDM2 (Figure 5A,C).

To test if the observed **19**-mediated MDM2(18−125) dimerization was unrelated to the lack of the N-terminal part of the MDM2 domain in the evaluated construct, we have solved the crystal structure of **19** in complex with a different construct of MDM2(1−125). Moreover, these crystals were obtained in different conditions and belonged to a different space group, providing a partial control of the influence of solvent conditions and crystal packing. Despite these differences, the dimerization mode within both structures is virtually identical, suggesting that dimer formation is compound induced rather than an effect of particular experimental conditions. The MDM2 molecules within the dimers seen in the two crystal forms align with RMSD of 0.198 Å for corresponding C_α atoms. The inhibitor dimers and interactions between the MDM2 molecules are also identical in both structures. The only difference is in amino acids 11−17, which were not present in the first construct but are present and defined by electron density in the second structure. This fragment closes the binding pocket from both sides of the dimer (Supporting Information, Figure S4) but has no significant effect on the mode of dimerization. Residues 1−10 were not defined by electron density.

Small molecule induced dimerization of MDM2 has already been previously reported by Graves et al. and by Surmiak et al., respectively, for RO-2443 (Roche, (*Z*)-5-((6-chloro-7-methyl-1*H*-indol-3-yl)methylene)-3-(3,4-difluorobenzyl)imidazolidine-2,4-dione, named hereafter **3.1**)[35] and 3-pyrrolin-2-ones/2-furanones.[36] In all instances, the dimer is mediated by direct interaction of the inhibitor moieties facing outside of the binding pocket of MDM2. However, when the structures of **19**, **3.1**, and 3-pyrrolin-2-ones/2-furanones induced dimers are

DOI: 10.1021/acs.jmedchem.7b00104
J. Med. Chem. 2017, 60, 4234−4244

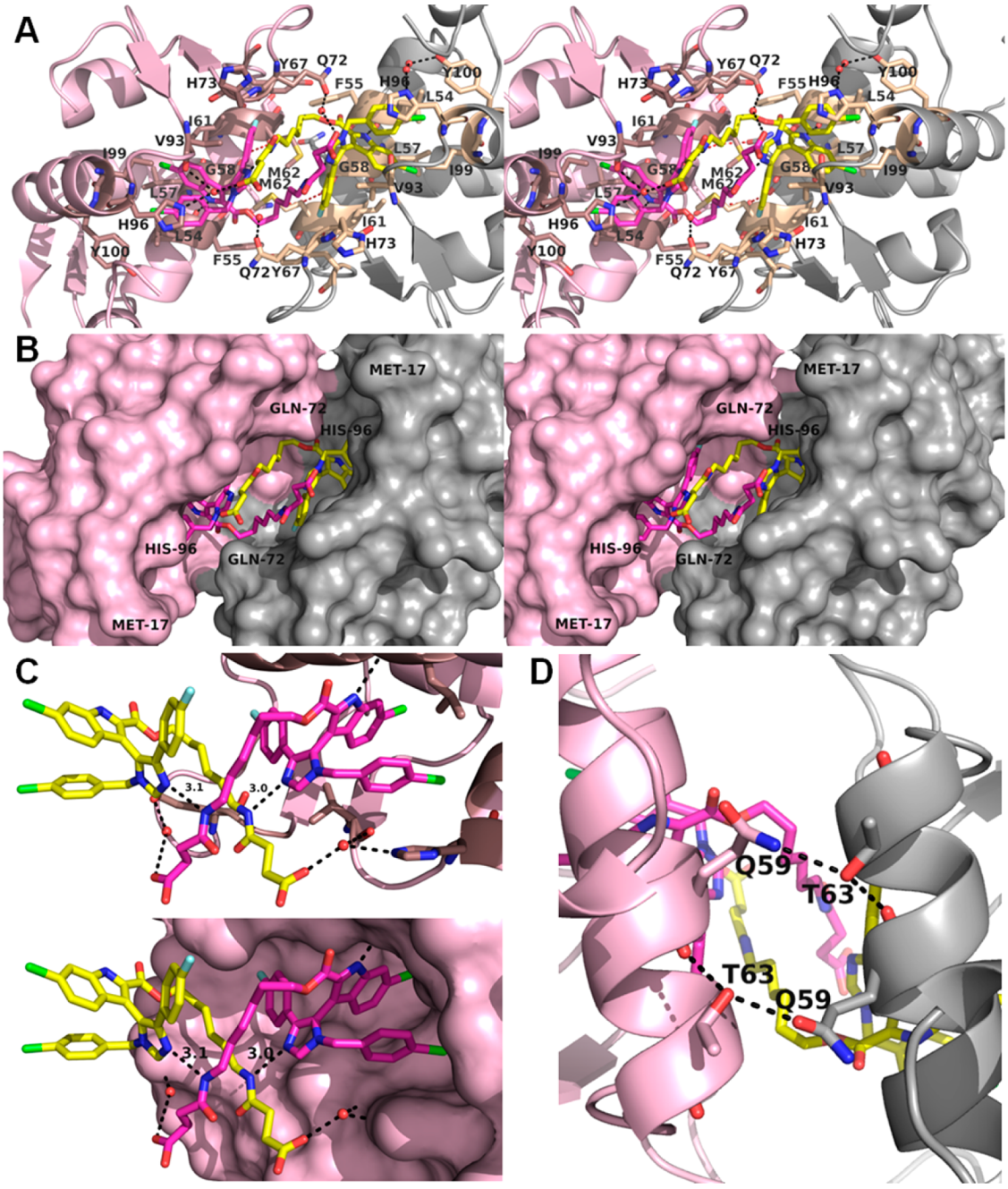

Figure 5. Crystal structure reveals the **19**-induced dimerization of MDM2. (A) Stereoview of the structure of the MDM2(18−125)−**19** complex. MDM2 chains A (pink) and B (gray) are shown in the cartoon representation. Inhibitors are shown as magenta and yellow sticks. Residues involved in the interactions with **19** are shown as sticks in salmon (chain A) or wheat (chain B) and labeled. Hydrogen bonds contributed by the inhibitors are depicted as black dashes. (B) Stereoview of the MDM2(18−125)−**19** complex, surface representation. Orientation and color coding same as in A. (C) Interinhibitor interactions: the close-up view of the MDM2 binding pocket shown as a pink cartoon (upper panel) or surface (lower panel) with the buried inhibitor molecule and adjacent inhibitor molecule. The second MDM2 molecule within the dimer is not shown. Hydrogen bonds are highlighted. (D) Direct protein−protein intermonomer interactions are formed between α-helices of the adjacent MDM2 molecules. The interacting residues are shown as sticks; hydrogen bonds are highlighted in black.

compared by aligning one of the MDM2 molecules within the dimer, the positions of the partner molecules do not significantly overlap, demonstrating different overall dimer arrangement (Supporting Information, Figures S5, S6). The interactions between the inhibitor molecules are also significantly different. In **19**, it is the amide within the linker of one inhibitor molecule that forms a hydrogen bond with the nitrogen of the imidazole ring of adjacent inhibitor and vice versa (Figure 5). In **3.1**, aromatic stacking between the indolyl-hydantoin groups of adjacent inhibitors is primarily involved (Supporting Information, Figure S5), whereas in 3-pyrrolin-2-ones/2-furanones, it is a water mediated interaction between the inhibitor molecules and a halogen bond formed by the inhibitor and adjacent protein molecule (Supporting Information, Figure S6).

Overall, although target protein dimerization through the interaction of exposed moieties of inhibitors is common for **19**, **3.1**, and 3-pyrrolin-2-ones/2-furanones, the detailed molecular

DOI: 10.1021/acs.jmedchem.7b00104
J. Med. Chem. 2017, 60, 4234−4244

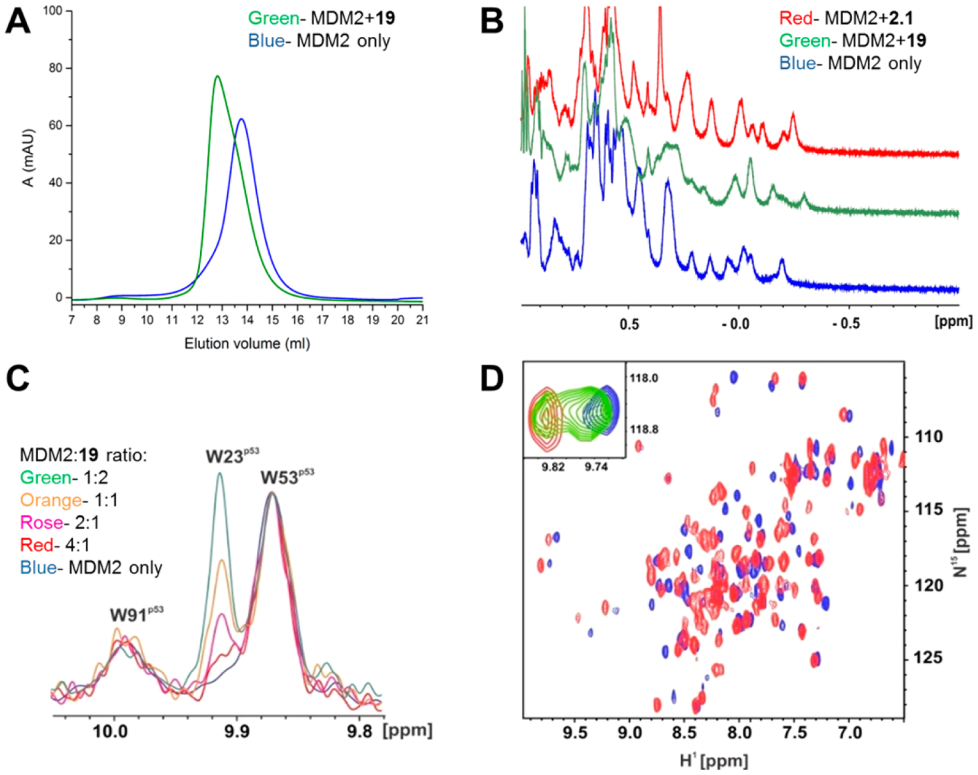

Figure 6. Compound **19** induces dimerization of MDM2 in solution and dissociates the MDM2−p53 complex. (A) Increased retention time of MDM2 in analytical gel filtration in the presence of **19** indicates formation of the dimer. (B) The aliphatic region of ^{1}H NMR spectra of MDM2(18−125) in the 1:1 complex with indicated compounds. **2.1** binds MDM2 but does not induce dimer formation. Broadening of NMR resonance peaks in the MDM2−**19** complex indicates the MDM2 dimerization. (C) One-dimensional AIDA NMR. The selected region of the 1D NMR spectrum is shown, containing resonances originating from W23, W53, and W91 of p53. The W23 peak is not present in the spectrum of the p53−MDM2 complex but is recovered after addition of **19**, indicating compound induced dissociation of the complex. (D) The HSQC spectrum of the ^{15}N-labeled MDM2 (blue) superimposed with the spectrum after addition of **16** in the 1:1 molar ratio (red). The inset shows an intermediate state of a selected peak at the MDM2:**16** molar ratio equal to 2:1 (green). NMR signal splitting indicates strong interaction at K_D below 1 μM.

mechanisms and the overall geometry of the resulting dimers are largely dissimilar.

19 Induces Dimerization of MDM2 in Solution and Dissociates p53−MDM2 Complex. The arrangement of the molecules in the crystal does not necessarily have to reflect the real biological assembly. Therefore, we evaluated if dimerization of MDM2 is induced by **19** in solution. The retention time characterizing MDM2 in analytical gel filtration decreased in the presence of **19**, indicating formation of higher molecular weight species, presumably dimers (based on column calibration with globular protein standard). **19**-induced shifts in the elution volume were observed for all MDM2 constructs evaluated in this study (1−118, 1−125, 18−125; Figure 6A; Supporting Information, Figure S7), so the observed dimerization is not induced by artificially exposing certain MDM2 surface.

Increase in the molecular mass of functional assembly results in increased relaxation time in NMR manifesting in signal broadening in the recorded spectra. To confirm **19**-induced dimerization of MDM2, the protein was titrated with the tested compound and the line width of well separated aliphatic signals in the region form −0.5 to 1.0 ppm of 1D ^{1}H NMR spectra was monitored. Line width changes were not observed upon titration with **2.1**, a reference compound known not to affect the monomeric state of MDM2 in solution. Titration with **19** resulted in marked broadening of peaks indicating the dimerization (Figure 6B, Supporting Information, Figure S7). Similar results were obtained regardless the MDM2 construct used (1−118, 18−125, and 1−125). These results further support the **19**-induced MDM2 dimerization in solution.

Next we asked if **19** is able to dissociate an existing p53−MDM2 complex. To test this, we employed a binding competition experiment, known as the 1D AIDA NMR (antagonist-induced dissociation assay).[37] The method relies on monitoring the line width changes associated with the changes in the molecular weight upon complex formation. The well separated, sharp signal originating from Trp23 of p53 transactivation domain broadens to the level of noise upon binding to MDM2. Displacement of p53 peptide from MDM2 complex by an MDM2 inhibitor results in the recovery of the specific signal in 1D ^{1}H NMR spectrum. Upon titration of p53−MDM2 complex with **19**, recovery of the specific Trp23 signal was observed, demonstrating that the compound effectively dissociates the p53−MDM2 interaction (Figure 6C), liberating p53 from the inhibition by its negative regulator.

CONCLUSIONS

Derivatization of the previously reported **1.1**, first into compound **1** and later by modification of the carboxyl moiety of the chloroindole scaffold, has led to a number of compounds with affinities comparable to the starting structure but characterized by significantly improved activity in cell-based assays. The best obtained compounds activated p53 in cancer cells to the level comparable to the golden standard, nutlin-3a, that is induced the cell cycle arrest, increased the expression of

DOI: 10.1021/acs.jmedchem.7b00104
J. Med. Chem. 2017, 60, 4234−4244

proapoptotic p21, and had a markedly increased cytotoxicity toward p53 positive cells. Crystal structure of an example compound (**19**) revealed a classical three-finger pharmacophore binding mode identical to that of **1.1**, but at the same time an unexpected, inhibitor induced dimerization of the target protein. The dimerization was confirmed in solution. Such unusual binding mode provides entirely new repertoire of optimization possibilities. Further, the long aliphatic linkers, containing functional groups, allow for future attachment of presented series of compounds to biological carriers (e.g., hyaluronic acid)[38] for improved pharmacodynamics and better delivery.

EXPERIMENTAL SECTION

Synthesis. Compounds **1** and **20**−**24** were obtained in the 3CR van Leusen reaction. **1** was further modified at position R_2 to obtain amide (**2**−**13**) and ester (**14**−**19**) derivatives using classical chemistry. The purity of all final compounds, determined by the chromatographic UPLC or elemental analysis, was 95% or higher. For details of synthesis and analysis, see the Supporting Information.

Protein Expression and Purification. Variants of the N-terminal domain of human MDM2 (1−118, 1−125, and 18−125) were cloned into the pET-20 (Novagen) and expressed in *Escherichia coli* strain BL21-CodonPlus(DE3)-RIL as described previously.[39] In brief, cells were cultured at 37 °C. Protein expression was induced with 1 mM IPTG at OD_{600} of 0.8 and cultured for additional 5 h at 37 °C. Cells were collected by centrifugation and lysed by sonication. Inclusion bodies were collected by centrifugation, washed with PBS containing 0.05% Triton-X100, and subsequently solubilized in 6 M guanidine hydrochloride in 100 mM Tris-HCl, pH 8.0, containing 1 mM EDTA and 10 mM β-mercaptoethanol. The protein was dialyzed against 4 M guanidine hydrochloride pH 3.5 supplemented with 10 mM β-mercaptoethanol. Following, the protein was refolded by dropwise addition into 10 mM Tris-HCl, pH 7.0, containing 1 mM EDTA and 10 mM β-mercaptoethanol and slow mixing overnight at 4 °C. Ammonium sulfate was added to the final concentration of 1.5 M, and the refolded protein was recovered on Butyl Sepharose 4 Fast Flow (GE Healthcare). The protein was eluted using 100 mM Tris-HCl pH 7.2 containing 5 mM β-mercaptoethanol and further purified by gel filtration on HiLoad 16/600 S75 (GE Healthcare) in 5 mM Tris-HCl pH 8.0 containing 50 mM NaCl and 5 mM β-mercaptoethanol (crystallization buffer) or in 50 mM phosphate buffer pH 7.4 containing 150 mM NaCl and 5 mM DTT (FP/NMR buffer).

N-Terminal domain of human MDMX (1−134) was cloned into pET-46Ek/LIC vector (Novagen). The vector was transformed into *Escherichia coli* strain BL21-CodonPlus(DE3)-RIL cells. The cells were cultured at 37 °C, and protein expression was induced with 0.5 mM IPTG at OD_{600} nm of 0.6. The recombinant protein expression was carried for 12 h at 20 °C. The protein was purified in native conditions by metal affinity chromatography. The preparation was polished by gel filtration on HiLoad 16/600 S75 (GE Healthcare) in 50 mM phosphate buffer pH 7.4 containing 150 mM NaCl and 5 mM DTT (FP/NMR buffer).

Fluorescence Polarization Assay. The assay was performed in 50 mM NaCl, 10 mM Tris pH 8.0, 1 mM EDTA containing 5% DMSO. To determine the optimal concentration of the protein for the competition binding assay, the effective concentration of MDM2 (1−118) and MDMX (1−134) was each time ascertained by determining the apparent K_d toward 5′FAM-LTFEHYWAQLTS (P2; 10 nM). Competition assay was performed by contacting serial dilutions of tested compounds with 10 nM P2 at protein concentration, yielding f_0 = 0.8.[40] Fluorescence polarization was determined at 485 nm excitation and 535 nm emission 15 min after mixing all assay components. All tests were performed using Corning black 96-well NBS assay plates at room temperature.

Cell Lines and Treatment with Compounds. U-2 OS ($p53^{wt}$), HCT 116 ($p53^{wt}$), and Saos-2 ($p53^{-/-}$) cells were cultured as monolayers in McCoy's 5A medium containing L-glutamine (Lonza) and supplemented with 10% fetal bovine serum (Biowest) at 37 °C and 5% CO_2 in a humidified atmosphere. All compounds were prepared as 50 mM stock solutions in DMSO. The cells were exposed to the inhibitors for indicated time periods. In each experiment, the final concentration of DMSO was kept constant and below detectable effect level.

Western Blot Analysis. U-2 OS cells and HCT 116 cells (120000 cells per well) were seeded on 12-well transparent plates (Falcon). The inhibitors were added 24 h following seeding, and the cells were cultured for additional 7 or 24 h. Cells were lysed with RIPA buffer (Sigma) supplemented with protease inhibitor cocktail (Sigma). The protein lysate was clarified by centrifugation and analyzed on 12% SDS polyacrylamide gel (Bio-Rad). The proteins were transferred to PVDF membrane (Merck Millipore). The membranes were blocked for 1 h in 5% BSA (Bioshop) in TTBS (100 mM Tris-HCl pH 8.0 containing 0.05% Tween-20 and 150 mM NaCl). Blots were probed with following antibodies: anti-MDM2 (Thermo Fisher Scientific, catalogue no. 700555), p21 (Cell Signaling, catalogue no. 2947), both at 1:2000 dilution, anti-p53 (Santa Cruz Biotechnology, catalogue no. sc-6243) at 1:200 dilution, or anti-GAPDH (Cell Signaling, catalogue no. 2118) at 1:3000 dilution. Antirabbit antibody conjugated with horseradish peroxidase (Cell Signaling, catalogue no. 7074) at 1:3000 dilution was used to detect the primary antibodies. The blots were developed using ECL Western Blotting Kit (Bio-Rad) and visualized using ChemiDoc System (Bio-Rad). Densitometric analysis was performed using ImageLab software (Bio-Rad).

Cell Viability Assay. U-2 OS cells (500 cells per well) and Saos-2 cells (1500 cells per well) were seeded on 96-well transparent plates (Falcon). Cells were treated with inhibitors 24 h following the seeding and cultured for additional 5 days. Thiazolyl blue tetrazolium bromide (MTT) was added at the final concentration of 500 ng mL^{-1}, and the cells were incubated for 1 h at 37 °C. The medium was removed, and formazan crystals were dissolved in 2-propanol containing 40 mM HCl. Absorbance was determined at 570 nm relative to 650 nm reference. Data was normalized to DMSO-treated control. Data was analyzed using Origin software (OriginLab). IC_{50} values were calculated by fitting of "Dose Resp" curves to experimental data sets.

Cell Cycle Analysis. U-2 OS cells were seeded at 300000 per 60 mm × 15 mm cell culture dish (Eppendorf), treated with tested inhibitors for 24 h, trypsinized, and fixed with 70% ethanol. The cell concentration was adjusted to 1×10^6 cells/sample, and DNA was labeled with PI-RNase solution (PBS, 5 μg mL^{-1} propidium iodide, 0.01 mg mL^{-1} RNase A) for 30 min at 25 °C. The cells analyzed for cell cycle DNA content using LSRFortessa cell analyzer (BD Biosciences).

Crystal Structure Determination. Human MDM2 (residues 18−125 and 1−125) was prepared in 5 mM Tris-HCl pH 8.0 containing 50 mM NaCl and 5 mM β-mercaptoethanol. Molar excess (3×) of **19** was added, and the complex was concentrated to 20 mg mL^{-1}. Screening for crystallization conditions was performed using sitting drop vapor diffusion setup and commercially available buffer sets (Qiagen, Hampton Research). Crystals of the MDM2(18−125)−**19** complex appeared after few days at 4 °C in 0.1 M Na HEPES pH 7.5 containing 10% 2-propanol and 20% PEG 4000. The MDM2(1−125)−**19** complex crystallized at 4 °C in 0.1 M HEPES pH 7.5 containing 0.2 M NaCl and 25% PEG 3350. The data collection and refinement description and statistics (Supporting Information, Table S6) are summarized in the Supporting Information.

Analytical Gel Filtration. MDM2(18−125, 1−118, and 1−125) at 1 mg mL^{-1} was contacted with 3× molar excess of tested inhibitor for 30 min, and the distribution on different molecular weight species was analyzed by gel filtration in the crystallization buffer using S75 10/300 GL column (GE Healthcare).

NMR Experiments. All NMR spectra were acquired at 300 K using a Bruker Avance 600 MHz spectrometer. Uniform ^{15}N isotope labeling was achieved by expression of the protein in the M9 minimal medium containing $^{15}NH_4Cl$ as the sole nitrogen source. MDM2(1−118)[41,42] was prepared in 50 mM phosphate buffer pH 7.4 containing 150 mM NaCl and 5 mM DTT. Then 10% (v/v) of D_2O was added to the samples to provide lock signal. Water suppression was carried out

DOI: 10.1021/acs.jmedchem.7b00104
J. Med. Chem. 2017, 60, 4234−4244

using the WATERGATE sequence.[43] Stock solutions of inhibitors used for titration were prepared in DMSO-d_6. The spectra were processed with TopSpin 3.2 software. $^{1}H-^{15}N$ heteronuclear correlations were obtained using the fast HSQC pulse sequence.[44] Assignment of the amide groups of MDM2 was obtained after ref 45. The AIDA experiments were performed according to ref 37.

■ ASSOCIATED CONTENT

Supporting Information

The Supporting Information is available free of charge on the ACS Publications website at DOI: 10.1021/acs.jmedchem.7b00104.

Details on chemical synthesis of compounds, X-ray, FP, and NMR (PDF)

Molecular formula strings(CSV)

Accession Codes

The final models and structure factors for MDM2−**19** complexes were deposited into Protein Data Bank with the following accession numbers: 5J7G (MDM2 18−125) and 5J7F (MDM2 1−125).

■ AUTHOR INFORMATION

Corresponding Authors

*For T.A.H.: phone, +48 126632287; E-mail, holak@biochem.mpg.de.

*For L.S.: phone, +48 126632041; E-mail, lukasz.skalniak@uj.edu.pl.

ORCID

Constantinos G. Neochoritis: 0000-0001-5098-5504

Alexander Dömling: 0000-0002-9923-8873

Lukasz Skalniak: 0000-0002-6707-6697

Tad A. Holak: 0000-0001-9369-6024

Author Contributions

#A. Twarda-Clapa, S. Krzanik, and K. Kubica contributed equally to this work.

Notes

The authors declare no competing financial interest.

■ ACKNOWLEDGMENTS

This research has been supported (to T. A. Holak) by the Maestro grant UMO-2012/06/A/ST5/00224 from the National Science Centre, Poland, by the project operated within the Foundation for Polish Science TEAM Program, cofinanced by the EU European Regional Development Fund and the Marie Curie FP7-Reintegration-Grant within the seventh European Community Framework Programme and (to G. Dubin) UMO-2011/01/D/NZ1/01169 from the National Science Centre. A. Twarda-Clapa was supported by Preludium grant UMO-2015/17/N/NZ1/00025, K. Kubica by Preludium grant UMO-2015/17/N/ST5/01942, L. Skalniak by Sonata grant UMO-2016/21/D/NZ7/00596, G. Dubin by Sonata bis grant UMO-2012/07/E/NZ1/01907 from the National Science Centre, Poland. A. Dömling was supported by the NIH (1R21GM087617, 1R01GM097082, and 1P41GM094055). The research was carried out with the equipment purchased thanks to the financial support of the European Union structural funds (contract nos. POIG.02.01.00-12-064/08 and POIG.02.01.00-12-167/08) and European Regional Development Fund in the framework of the Polish Innovation Economy Operational Program (contract no. POIG.02.01.00-12-023/08). This project has received funding from the European Union's Framework Programme for Research and Innovation Horizon 2020 (2014−2020) under the Marie Skłodowska-Curie Grant Agreement no. 675555, Accelerated Early staGe drug discovery (AEGIS). S. Krzanik and A. Twarda-Clapa received the financial support from the Faculty of Biochemistry, Biophysics, and Biotechnology of Jagiellonian University, a partner of the Leading National Research Center (KNOW) supported by the Ministry of Science and Higher Education.

■ ABBREVIATIONS USED

3CR, 3-component reaction; AIDA, antagonist-induced dissociation assay; FP, fluorescence polarization; GAPDH, glyceraldehyde-3-phosphate dehydrogenase; MTT, 3-(4,5-dimethylthiazol-2-yl)-2,5-diphenyltetrazolium bromide; MDM2, murine double minute-2; MDMX, murine double minute-X; PVDF, polyvinylidene fluoride; RMSD, root mean square deviation

■ REFERENCES

(1) Brown, C. J.; Lain, S.; Verma, C. S.; Fersht, A. R.; Lane, D. P. Awakening guardian angels: drugging the p53 pathway. *Nat. Rev. Cancer* **2009**, *9*, 862−873.

(2) Cheok, C. F.; Verma, C. S.; Baselga, J.; Lane, D. P. Translating p53 into the clinic. *Nat. Rev. Clin. Oncol.* **2011**, *8*, 25−37.

(3) Wade, M.; Li, Y. C.; Wahl, G. M. MDM2, MDMX and p53 in oncogenesis and cancer therapy. *Nat. Rev. Cancer* **2013**, *13*, 83−96.

(4) Hock, A. K.; Vousden, K. H. The role of ubiquitin modification in the regulation of p53. *Biochim. Biophys. Acta, Mol. Cell Res.* **2014**, *1843*, 137−149.

(5) Karni-Schmidt, O.; Lokshin, M.; Prives, C. The roles of MDM2 and MDMX in cancer. *Annu. Rev. Pathol.: Mech. Dis.* **2016**, *11*, 617−644.

(6) Gu, J.; Wang, B.; Liu, Y.; Zhong, L.; Tang, Y.; Guo, H.; Jiang, T.; Wang, L.; Li, Y.; Cai, L. Murine double minute 2 siRNA and wild-type p53 gene therapy interact positively with zinc on prostate tumours in vitro and in vivo. *Eur. J. Cancer* **2014**, *50*, 1184−1194.

(7) Shangary, S.; Qin, D.; McEachern, D.; Liu, M.; Miller, R. S.; Qiu, S.; Nikolovska-Coleska, Z.; Ding, K.; Wang, G.; Chen, J.; Bernard, D.; Zhang, J.; Lu, Y.; Gu, Q.; Shah, R. B.; Pienta, K. J.; Ling, X.; Kang, S.; Guo, M.; Sun, Y.; Yang, D.; Wang, S. Temporal activation of p53 by a specific MDM2 inhibitor is selectively toxic to tumors and leads to complete tumor growth inhibition. *Proc. Natl. Acad. Sci. U. S. A.* **2008**, *105*, 3933−3938.

(8) Miyachi, M.; Kakazu, N.; Yagyu, S.; Katsumi, Y.; Tsubai-Shimizu, S.; Kikuchi, K.; Tsuchiya, K.; Iehara, T.; Hosoi, H. Restoration of p53 pathway by nutlin-3 induces cell cycle arrest and apoptosis in human rhabdomyosarcoma cells. *Clin. Cancer Res.* **2009**, *15*, 4077−4084.

(9) Chen, L.; Rousseau, R. F.; Middleton, S. A.; Nichols, G. L.; Newell, D. R.; Lunec, J.; Tweddle, D. A. Pre-clinical evaluation of the MDM2-p53 antagonist RG7388 alone and in combination with chemotherapy in neuroblastoma. *Oncotarget* **2015**, *6*, 10207−10221.

(10) Feng, F. Y.; Zhang, Y.; Kothari, V.; Evans, J. R.; Jackson, W. C.; Chen, W.; Johnson, S. B.; Luczak, C.; Wang, S.; Hamstra, D. A. MDM2 inhibition sensitizes prostate cancer cells to androgen ablation and radiotherapy in a p53-dependent manner. *Neoplasia* **2016**, *18*, 213−222.

(11) Vassilev, L. T.; Vu, B. T.; Graves, B.; Carvajal, D.; Podlaski, F.; Filipovic, Z.; Kong, N.; Kammlott, U.; Lukacs, C.; Klein, C.; Fotouhi, N.; Liu, E. A. In vivo activation of the p53 pathway by small-molecule antagonists of MDM2. *Science* **2004**, *303*, 844−848.

(12) Hoe, K. K.; Verma, C. S.; Lane, D. P. Drugging the p53 pathway: understanding the route to clinical efficacy. *Nat. Rev. Drug Discovery* **2014**, *13*, 217−236.

(13) Zhao, Y.; Aguilar, A.; Bernard, D.; Wang, S. Small-molecule inhibitors of the MDM2-p53 protein-protein interaction (MDM2

DOI: 10.1021/acs.jmedchem.7b00104
J. Med. Chem. 2017, 60, 4234−4244

Inhibitors) in clinical trials for cancer treatment. *J. Med. Chem.* **2015**, *58*, 1038−1052.
(14) Burgess, A.; Chia, K. M.; Haupt, S.; Thomas, D.; Haupt, Y.; Lim, E. Clinical overview of MDM2/X-targeted therapies. *Front. Oncol.* **2016**, *6*, 7.
(15) Urso, L.; Calabrese, F.; Favaretto, A.; Conte, P.; Pasello, G. Critical review about MDM2 in cancer: Possible role in malignant mesothelioma and implications for treatment. *Crit Rev. Oncol Hematol.* **2016**, *97*, 220−230.
(16) Popowicz, G. M.; Dömling, A.; Holak, T. A. The structure-based design of Mdm2/Mdmx-p53 inhibitors gets serious. *Angew. Chem., Int. Ed.* **2011**, *50*, 2680−2688.
(17) Uversky, V. N.; Dave, V.; Iakoucheva, L. M.; Malaney, P.; Metallo, S. J.; Pathak, R. R.; Joerger, A. C. Pathological unfoldomics of uncontrolled chaos: intrinsically disordered proteins and human diseases. *Chem. Rev.* **2014**, *114*, 6844−6879.
(18) Milroy, L. G.; Grossmann, T. N.; Hennig, S.; Brunsveld, L.; Ottmann, C. Modulators of protein−protein interactions. *Chem. Rev.* **2014**, *114*, 4695−4748.
(19) Pelay-Gimeno, M.; Glas, A.; Koch, O.; Grossmann, T. N. Structure-based design of inhibitors of protein-protein interactions: mimicking peptide binding epitopes. *Angew. Chem., Int. Ed.* **2015**, *54*, 8896−8927.
(20) Kussie, P. H.; Gorina, S.; Marechal, V.; Elenbaas, B.; Moreau, J.; Levine, A. J.; Pavletich, N. P. Structure of the MDM2 oncoprotein bound to the p53 tumor suppressor transactivation domain. *Science* **1996**, *274*, 948−953.
(21) Joerger, A. C.; Fersht, A. R. The p53 pathway: origins, inactivation in cancer, and emerging therapeutic approaches. *Annu. Rev. Biochem.* **2016**, *85*, 375−404.
(22) Ding, K.; Lu, Y.; Nikolovska-Coleska, Z.; Qiu, S.; Ding, Y.; Gao, W.; Stuckey, J.; Krajewski, K.; Roller, P. P.; Tomita, Y.; Parrish, D. A.; Deschamps, J. R.; Wang, S. Structure-based design of potent non-peptide MDM2 inhibitors. *J. Am. Chem. Soc.* **2005**, *127*, 10130−10131.
(23) Ding, K.; Lu, Y.; Nikolovska-Coleska, Z.; Wang, G.; Qiu, S.; Shangary, S.; Gao, W.; Qin, D.; Stuckey, J.; Krajewski, K.; Roller, P. P.; Wang, S. Structure-based design of spiro-oxindoles as potent, specific small-molecule inhibitors of the MDM2-p53 interaction. *J. Med. Chem.* **2006**, *49*, 3432−3435.
(24) Michelsen, K.; Jordan, J. B.; Lewis, J.; Long, A. M.; Yang, E.; Rew, Y.; Zhou, J.; Yakowec, P.; Schnier, P. D.; Huang, X.; Poppe, L. Ordering of the N-terminus of human MDM2 by small molecule inhibitors. *J. Am. Chem. Soc.* **2012**, *134*, 17059−17067.
(25) Vogel, S. M.; Bauer, M. R.; Joerger, A. C.; Wilcken, R.; Brandt, T.; Veprintsev, D. B.; Rutherford, T. J.; Fersht, A. R.; Boeckler, F. M. Lithocholic acid is an endogenous inhibitor of MDM4 and MDM2. *Proc. Natl. Acad. Sci. U. S. A.* **2012**, *109*, 16906−16910.
(26) Bista, M.; Wolf, S.; Khoury, K.; Kowalska, K.; Huang, Y.; Wrona, E.; Arciniega, M.; Popowicz, G. M.; Holak, T. A.; Dömling, A. Transient protein states in designing inhibitors of the MDM2-p53 interaction. *Structure* **2013**, *21*, 2143−2151.
(27) Baek, S.; Kutchukian, P. S.; Verdine, G. L.; Huber, R.; Holak, T. A.; Lee, K. W.; Popowicz, G. M. Structure of the stapled p53 peptide bound to Mdm2. *J. Am. Chem. Soc.* **2012**, *134*, 103−106.
(28) Chang, Y. S.; Graves, B.; Guerlavais, V.; Tovar, C.; Packman, K.; To, K. H.; Olson, K. A.; Kesavan, K.; Gangurde, P.; Mukherjee, A.; Baker, T.; Darlak, K.; Elkin, C.; Filipovic, Z.; Qureshi, F. Z.; Cai, H.; Berry, P.; Feyfant, E.; Shi, X. E.; Horstick, J.; Annis, D. A.; Manning, A. M.; Fotouhi, N.; Nash, H.; Vassilev, L. T.; Sawyer, T. K. Stapled α-helical peptide drug development: a potent dual inhibitor of MDM2 and MDMX for p53-dependent cancer therapy. *Proc. Natl. Acad. Sci. U. S. A.* **2013**, *110*, E3445−E3454.
(29) Popowicz, G. M.; Czarna, A.; Wolf, S.; Wang, K.; Wang, W.; Dömling, A.; Holak, T. A. Structures of low molecular weight inhibitors bound to MDMX and MDM2 reveal new approaches for p53-MDMX/MDM2 antagonist drug discovery. *Cell Cycle* **2010**, *9*, 1104−1111.
(30) Dömling, A.; Wang, W.; Wang, K. Chemistry and biology of multicomponent reactions. *Chem. Rev.* **2012**, *112*, 3083−3135.
(31) Skinner, A. L.; Laurence, J. S. High-field solution NMR spectroscopy as a tool for assessing protein interactions with small molecule ligands. *J. Pharm. Sci.* **2008**, *97*, 4670−4695.
(32) Powers, R. Advances in nuclear magnetic resonance for drug discovery. *Expert Opin. Drug Discovery* **2009**, *4*, 1077−1098.
(33) Dömling, A. Small molecular weight protein−protein interaction antagonists—an insurmountable challenge? *Curr. Opin. Chem. Biol.* **2008**, *12*, 281−291.
(34) Ding, Q.; Zhang, Z.; Liu, J.-J.; Jiang, N.; Zhang, J.; Ross, T. M.; Chu, X.-J.; Bartkovitz, D.; Podlaski, F.; Janson, C.; Tovar, C.; Filipovic, Z. M.; Higgins, B.; Glenn, K.; Packman, K.; Vassilev, L. T.; Graves, B. Discovery of RG7388, a potent and selective p53-MDM2 inhibitor in clinical development. *J. Med. Chem.* **2013**, *56*, 5979−5983.
(35) Graves, B.; Thompson, T.; Xia, M.; Janson, C.; Lukacs, C.; Deo, D.; Di Lello, P.; Fry, D.; Garvie, C.; Huang, K. S.; Gao, L.; Tovar, C.; Lovey, A.; Wanner, J.; Vassilev, L. T. Activation of the p53 pathway by small-molecule-induced MDM2 and MDMX dimerization. *Proc. Natl. Acad. Sci. U. S. A.* **2012**, *109*, 11788−11793.
(36) Surmiak, E.; Twarda-Clapa, A.; Zak, K. M.; Musielak, B.; Tomala, M. D.; Kubica, K.; Grudnik, P.; Madej, M.; Jablonski, M.; Potempa, J.; Kalinowska-Tluscik, J.; Dömling, A.; Dubin, G.; Holak, T. A. A Unique Mdm2-binding mode of the 3-pyrrolin-2-one- and 2-furanone-based antagonists of the p53-Mdm2 interaction. *ACS Chem. Biol.* **2016**, *11*, 3310−3318.
(37) Bista, M.; Kowalska, K.; Janczyk, W.; Dömling, A.; Holak, T. A. Robust NMR screening for lead compounds using tryptophan-containing proteins. *J. Am. Chem. Soc.* **2009**, *131*, 7500−7501.
(38) Oh, E. J.; Park, K.; Kim, K. S.; Kim, J.; Yang, J. A.; Kong, J. H.; Lee, M. Y.; Hoffman, A. S.; Hahn, S. K. Target specific and long-acting delivery of protein, peptide, and nucleotide therapeutics using hyaluronic acid derivatives. *J. Controlled Release* **2010**, *141*, 2−12.
(39) Czarna, A.; Popowicz, G. M.; Pecak, A.; Wolf, S.; Dubin, G.; Holak, T. A. High affinity interaction of the p53 peptideanalogue with human Mdm2 and Mdmx. *Cell Cycle* **2009**, *8*, 1176−1184.
(40) Huang, X. Fluorescence polarization competition assay: the range of resolvable inhibitor potency is limited by the affinity of the fluorescent ligand. *J. Biomol. Screening* **2003**, *8*, 34−38.
(41) Showalter, S. A.; Bruschweiler-Li, L.; Johnson, E.; Zhang, F.; Brüschweiler, R. Quantitative lid dynamics of Mdm2 reveals differential ligand binding modes of the p53-binding cleft. *J. Am. Chem. Soc.* **2008**, *130*, 6472−6478.
(42) Grace, C. R.; Ban, D.; Min, J.; Mayasundari, A.; Min, L.; Finch, K. E.; Griffiths, L.; Bharatham, N.; Bashford, D.; Kiplin Guy, R.; Dyer, M. A.; Kriwacki, R. W. Monitoring ligand-induced protein ordering in drug discovery. *J. Mol. Biol.* **2016**, *428*, 1290−1303.
(43) Piotto, M.; Saudek, V.; Sklenár, V. Gradient-tailored excitation for single-quantum NMR spectroscopy of aqueous solutions. *J. Biomol. NMR* **1992**, *2*, 661−665.
(44) Mori, S.; Abeygunawardana, C.; Johnson, M. O.; van Zijl, P. C. Improved sensitivity of HSQC spectra of exchanging protons at short interscan delays using a new fast HSQC (FHSQC) detection scheme that avoids water saturation. *J. Magn. Reson., Ser. B* **1995**, *108*, 94−98.
(45) Stoll, R.; Renner, C.; Hansen, S.; Palme, S.; Klein, C.; Belling, A.; Zeslawski, W.; Kamionka, M.; Rehm, T.; Muhlhahn, P.; Schumacher, R.; Hesse, F.; Kaluza, B.; Voelter, W.; Engh, R. A.; Holak, T. A. Chalcone derivatives antagonize interactions between the human oncoprotein MDM2 and p53. *Biochemistry* **2001**, *40*, 336−344.

DOI: 10.1021/acs.jmedchem.7b00104
J. Med. Chem. 2017, 60, 4234−4244